

Rock physics template (RPT) analysis of well logs and seismic data for lithology and fluid classification in Cambay Basin

Saurabh Datta Gupta · Rima Chatterjee ·
M. Y. Farooqui

Received: 9 November 2010 / Accepted: 12 November 2011 / Published online: 5 January 2012
© Springer-Verlag 2012

Abstract The Cambay Basin is 450-km-long north–south-trending graben with an average width of 50 km, having maximum depth of about 7 km. The origin of the Cambay and other Basins on the western margin of India are related to the break up of the Gondwana super-continent in the Late-Triassic to Early-Jurassic (215 ma). The structural disposition of the Pre-Cambrian basement—a complex of igneous and metamorphic rocks exposed in the vicinity of the Cambay Basin—controls its architecture. The principal lineaments in the Basin are aligned towards NE-SE, ENE-WSW and NNW-SSE, respectively. Rock physics templates (RPTs) are charts and graphs generated by using rock physics models, constrained by local geology, that serve as tools for lithology and fluid differentiation. RPT can act as a powerful tool in validating hydrocarbon anomalies in undrilled areas and assist in seismic interpretation and prospect evaluation. However, the success of RPT analysis depends on the availability of the local geological information and the use of the proper model. RPT analysis has been performed on well logs and seismic data of a particular study area in mid Cambay Basin. Rock physics diagnostic approach is adopted in the study area placed at mid Cambay Basin to estimate the volume in the reservoir sands from 6 wells (namely; A, B, C, D, E and F) where oil was already encountered in one well, D.

In the study area, hydrocarbon prospective zone has been marked through compressional (P wave) and shear wave (S wave) impedance only. In the RPT analysis, we have plotted different kinds of graphical responses of Lamé's parameters, which are the function of P-wave velocity, S-wave velocity and density. The discrete thin sand reservoirs have been delineated through the RPT analysis. The reservoir pay sand thickness map of the study area has also been derived from RPT analysis and fluid characterization. Through this fluid characterization, oil-bearing thin sand layers have been found in well E including well D. The sand distribution results prove that this methodology has able to perform reservoir characterization and seismic data interpretation more quantitatively and efficiently.

Keywords Rock physics template · Cambay Basin · Seismic inversion · Fluid substitution · Reservoir characterization

Introduction

Rock physics deals with the relationship between measurements of elastic parameters made from the surface, well, laboratory equipment and intrinsic physical and chemical properties of the rocks (Sayers 2009). To analyse the elastic properties [velocity, density, impedance, and ratio of P wave velocity (V_p) and S-wave velocity (V_s)] rock physics knowledge is required (Avseth 2000), which acts as a bridge that links the elastic properties to the reservoir properties such as water saturation, porosity and shale volume. The reservoir parameters such as porosity, lithofacies, pore fluid type, saturation and pore pressure can be very well understood with the help of rock physics and these are directly or indirectly sensible to the seismic velocity of the subsurface

S. Datta Gupta (✉) · M. Y. Farooqui
Gujarat State Petroleum Corporation Limited,
Gandhinagar 382010, Gujarat, India
e-mail: saurabh.doc.ism@gmail.com; saurabhd@gspc.in

M. Y. Farooqui
e-mail: farooqui@gspc.in

R. Chatterjee
Department of Applied Geophysics, Indian School of Mines,
Dhanbad 826004, Jharkhand, India
e-mail: rima_c_99@yahoo.com

formation. Thus, rock physics can be applied to predict reservoir parameters, such as lithologies and pore fluids from seismically derived attributes, especially in undrilled Areas and thereby reducing exploration risks.

Rock physics models, constrained by local geology, can be used to prepare charts or graphs for prediction of lithology and hydrocarbons. These locally constrained charts or Basin-specific rock physics models are known as *Rock Physics Templates* or simply RPTs (Ødegaard and Avseth 2004). Geologic constraints on rock physics templates include lithology, mineralogy, burial depth, diagenesis (cementation), pressure and temperature. In general, it is essential to include only the expected lithologies for the area under investigation when generating the templates (Avseth et al. 2005). The common form of RPT is between acoustic impedance (AI) (product of rock density and p-wave velocity) and V_p/V_s ratio, as combination of these two elastic properties is a good lithology and fluid indicator (Avseth et al. 2005; Chi and Han 2009). Other forms of RPT include combination of shear impedance (SI) and AI, elastic impedance (EI) and AI, Lamé's parameter (λ) and shear modulus (μ), matrix and fluid indicator ($\lambda * \rho$) and matrix indicator ($\mu * \rho$), etc. The all kind of geo-scientific data includes combination of seismic and well log data. The RPT technology has a wide range of application ranging from analysis and quality control of seismic inversion results to formation evaluation. However, the reliability of the templates depends on the quality of the input data and the model assumptions. The important requirements for RPTs are information about the local geology like depositional environment and sedimentology: diagenesis or cementation, sorting trend, compaction, etc. Detailed mineralogy of the rocks and other information's include pore fluid saturation, properties of mud filtrate (for well log data), properties of formation water and hydrocarbons, pressure, temperature and brine salinity. Figure 1 (Brie et al. 1995) shows an example of a rock physics template where different geological trends can be identified. When the field data are superimposed on the template, the data points can be clustered into different groups and accordingly classified as different facies (Mavko et al. 1998).

Geology of the study area

The major structural setting of this area and its immediate surrounding areas can be broadly defined as follows (Balakrishnan et al. 1977):

- A NNW—SSE-trending basement ridge (Palaeocene-Lower Eocene).
- The Kauka-Wataman Sub-Basin immediately west of the ridge. This sub-Basin is bound to the west by the Wataman-Baola Basin-Bounding fault.

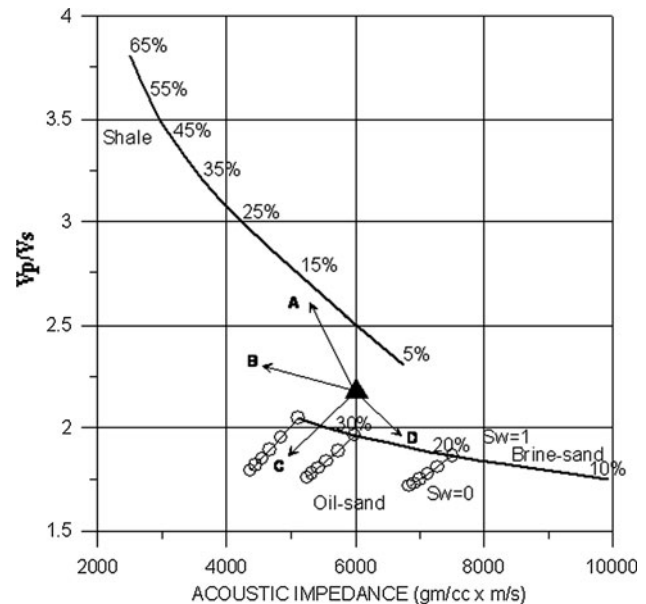


Fig. 1 Showing P-impedance versus V_p/V_s cross-plot for lithology identification (after Ødegaard and Avseth 2004)

- Further to the west of this bounding fault is the Wataman Rupwati High.
- To the north of the ridge lies the southern extension of Vasnakeliya Ambheti sub-Basin.
- The southern half of the ridge is surrounded by the Tarapur depression in the east and south.

Stratigraphy and depositional environment of the study area

From the 3D seismic and well data, the stratigraphy of the study area can be well constructed (Balakrishnan et al. 1977). The formations encountered from bottom as well as comprehensive descriptions of individual litho units observed from cores, well cuttings and master log (not being available at present) have been described below.

Deccan trap

This formation is comprised of several lava flows that took place during Upper Cretaceous; fourteen numbers of such flows have been recognized in the basin, separated by thin inter-trappean beds consisting of variegated claystone and pockets of calcite. In the study area, it appears that one such inter-trappean bed is represented by vesicular as well as non-vesicular basalts associated with Andesite, Trachyte and Picrite. Vesicles are filled with secondary minerals like Calcite, Zeolite and Silica and occasionally, Kaolinised Feldspar. This unit forms the technical/economic basement for this Area.

Olpad formation

It is comprised of volcanic conglomerates, sandstone, silt, shale, claystone and clays mainly derived from Deccan Trap highs. This formation exhibits varying colour shades from light grey to dark brown or even flaming red.

Three lithosomes are seen in this formation with varying degrees of inter-mix:

- Upper—Sandstone
- Middle—Claystone
- Lower—Trapwash

On the basis of 3D seismic, log motifs and lithological description, it has been inferred that Olpad formation might have deposited under a freshwater to slightly brackish water environment. The poorly sorted nature and predominance of angular to subangular sediments suggest that sediments were transported under high energy conditions and deposited directly adjacent to the Deccan Trap highs. This very nature of the sediments studied from the FMI log further suggests that they were transported from source area to alluvial fans by stream channels. The inter-layered finer clastics indicate their deposition along the banks of the channels.

In the conglomerate, the trap fragments occur as angular to subrounded pebbles, gravels, sands and silts and do not show any selective sorting. The sands are very fine to medium grained, and their matrix is clayey and chloritic, derived from trap terrain, and showing diagenetic alterations. It has been reported in technical literature that conglomerates deposited on alluvial fans (fanglomerates) gave rise to finer-grained rocks, some with secondary porosity due to leaching and fracturing (Banerjee et al. 2002). Reservoirs of a commercial nature have been encountered in this formation in this area.

Cambay shale

The formation is mainly composed of black fissile shale, pyritic and rich in combined organic matter with minor silt streaks. The sequence does not contain coarse clastics except locally. However, occasionally, calcareous silts are developed in the lower portion (Older Cambay Shale) and coarse clastics in the upper portion (Younger Cambay Shale). Older Cambay Shale formation is interpreted to have been laid down in a rapidly sinking Basin with, generally speaking, high stand conditions. Preservation of organic matter in the Lower Cambay Shale on account of rapid burial due to the high rate of sedimentation may be responsible for the hydrocarbons generated in the area. Within the Younger Cambay shale, a typical development of arenaceous facies equivalent to Dholka Middle pays has been observed. These have been locally termed as DJP-1 in the Wataman-Kauka sub-Basin and DJP-2 on the ridge.

Kalol formation

It is generally composed of alterations of sandstone, siltstone, shale, sideritic claystone and coal. The carbonaceous shales are grey to dark grey coloured. In this area, however, the sandstones are less developed, and oolitic sediments are more prevalent. The occurrence of oolites is a typical feature of this part of the Basin, reflecting a shallow estuarine or tidal flat environment with limited sediment supply, moderate agitation and redox conditions—distal of the main Kalol Delta front. These oolites are rounded bodies of ferruginous, clayey and siliceous matter. As stated earlier, since the depositional control was by the Kalol Delta, its extent was limited to the north of the study area.

Tarapur formation

It is extensive throughout this part of the Basin and is generally characterized by greenish grey to dray grey, light brown, soft to moderately hard, poorly fissile shale, with thin, silty sideritic bands in the lower part. This formation was laid down in a primarily marine environment in this area.

Neogene and quaternary sequences

The base of these formations—Babaguru—lies unconformably over the preceding Tarapur formation top. They are comprised, from below, of clays/claystones, sands/claystones, clays and a covering of ill-sorted alluvium (Kundu and Wani 1992). The depositional environments generally represented here are shallow water up to Miocene and fluvial above.

Objectives

Seismic inversion techniques invert P-waves or converted wave seismic data and/or gathers into different elastic parameters such as acoustic impedance, shear wave impedance, elastic impedance, density, velocity ratio and Poisson's ratio. This elastic parameters have been linked to the rock properties (such as lithology, porosity and pore fluids), which can be further used for reservoir characterization and fluids identification (Avseth et al. 2005; Fatti et al. 1994; Gray et al. 1999; He et al. 2011; Xu and Payne 2009). Integrating core data, well log and seismic data, the rock physics analysis aims to study the effects of rock physical parameter changes (such as lithologic character, porosity, pore texture, fluid type and saturation) on rock elastic properties (He et al. 2011). In this paper, rock physical properties using seismic responses and the related

changes of seismic attributes has been investigated. An attempt has also been taken to build RPT for an unconventional tight thin sand reservoir in the Cambay Basin, India, to guide seismic inversion interpretation results for reservoir characterization and fluids identification purpose.

The study area is located in the mid onshore Cambay Basin in Western India (Fig. 2). The six wells namely A, B, C, D, E and F located in the study area penetrate a reasonably thick section of Recent, Miocene and Oligocene sediments, where oil is already encountered in well D. The sediments are mainly composed of shales, silts and sandstones. Oil sands appear around the well with an average porosity of about 15%, beneath a cap rock of silty-shale. This is followed by a section of Eocene sandstones and shales, with thin Pay zones of sideritic sands, which are oolitic in nature and separated by laminae of silts and muds. The thick Cambay Shale marks the beginning of this Eocene section. Deeper in the section, the wells penetrate the Palaeocene and composed of inter-bedded silts, sandstones and relatively thick shale sequences. Pay zones in this section are again largely composed of oolites (sideritic sand). The Deccan Traps with intra-volcanic Pay zones (thin volcanic sands and weathered volcanics/volcanoclastics) are underlying the sideritic pay sand.

The main objective of this study is to characterize the thin unconventional reservoir pay sand through (1)

inversion of partial-angle stack data to P-impedance and V_p/V_s , (2) computation of S-impedance, Lambda-Rho and Mu-Rho for RPT analysis, and (3) fluid characterization from P- and S-impedance volumes in the study area of mid Cambay Basin. The reservoir of the area is very tight; somewhere the pay sands are juxtaposed in between non-reservoir facies of unconventional reservoir formation. The subsurface sandstone formation is identified as being hydrocarbon-bearing when the measured V_p/V_s ratio in the subsurface formation is less than an identified minimum of the V_p/V_s ratios determined for water-bearing sandstone and shale. The addition of shear wave velocity interpretation would improve the imaging of hydrocarbon filled porosity and its discrimination from volcanics and shales in these processes.

Methodology

Following is a brief description of algorithms, which have been followed to meet the foregoing objectives in the study area of the mid Cambay Basin. Fugro Jason Geoscience Workbench (JSW) software and Ikon Science RokDoC have been used to carry out the RPT analysis. Seismic reflection/angle stack data, available interpreted seismic horizons, seismic velocity, well log and Formation tops have been considered as major input data set.

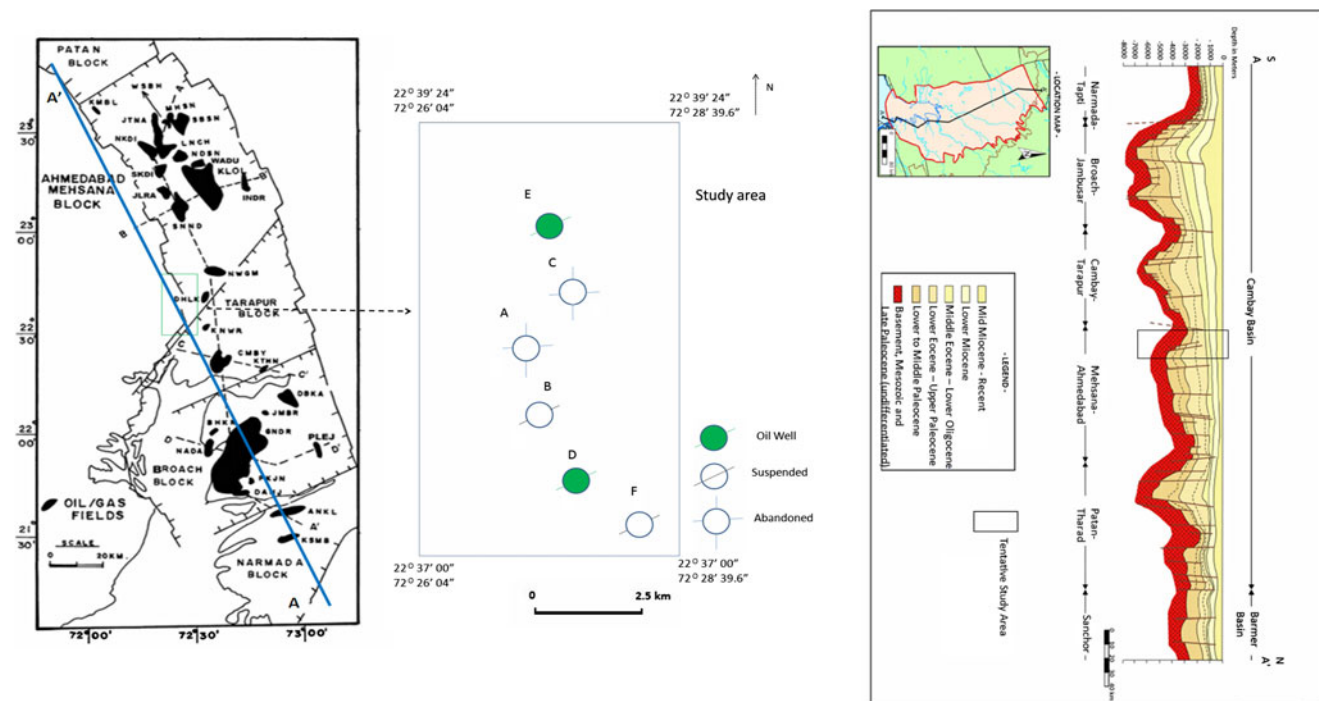


Fig. 2 Study area located at the Cambay Basin along with well location; Seismic Section is displayed across N–S of the Cambay Basin

Input data

Seismic data

Partial-angle stack seismic data have been considered for angle stack inversion. They covered the following angle ranges:

- Stack 1: 05–10°,
- Stack 2: 10–18°,
- Stack 3: 18–26°,
- Stack 4: 26–33°,
- Stack 5: 33–40°,
- Stack 6: 40–46° respectively.

To overcome the problem of angle coverage in some of the angle stacks, averaging of partial stacks have been undertaken.

- Averaging of Stack 1 and Stack 2
- Averaging of Stack 3 and Stack 4
- Averaging of Stack 5 and Stack 6

These arises additional seismic partial stacks as below:

- Stack 7: 05–18°
- Stack 8: 18–33°
- Stack 9: 33–46°

Good power spectra have been observed up to 90 Hz in the near stack but only to about 50 Hz on the far stack. The RMS seismic amplitude has been determined across the study between horizons Miocene Basal Sand and Oligocene for Stack 1 and Stack 8 (Davies and Portniaguine 2004). There are apparent acquisition edge effects in Stack 1 but these are reduced in the averaged Stack 8.

Horizon interpretation

The following formations are considered for the study area of mid Cambay Basin (Balakrishnan et al. 1977; Banerjee et al. 2002; Kundu and Wani 1992).

- Base Pliocene
- Miocene Basal Sand
- Oligocene
- Eocene Pay I
- Eocene Pay IV
- Kalol Base
- Dholka Middle Pay I
- Dholka Middle Pay 2
- Deccan Trap (Upper Cretaceous)

These horizons were smoothed and interpolated where necessary for use in the inversion workflow. The Deccan Trap horizon has been copied down by 500 ms to add another constraint surface to the inversion.

Log data

The availability of physical parameters [Vp (derived from P-sonic), Vs (derived from S-sonic and Density)] for six wells have been mentioned in below Table 1.

Log modelling for computation of elastic modulus

Prior to know the effect of elastic moduli on amplitude variation with offset (AVO), the logs may be checked to see whether they represent a set of self-consistent geophysical information. Effects due to cycle skipping, bad bore-hole and bad data regions are edited. Conventional wisdom holds that the sonic log is relatively unaffected by poor hole conditions. Most log analysis programs by default use the sonic log for porosity determination where borehole conditions are bad. In rugose hole, the sonic log may appear to be satisfactory with some cycle-skips. However, these first impressions of sonic log accuracy may be misleading. It is then possible to fill in missing or bad data with log information from rock physics using Xu and White's model (Xu and White 1995) and Greenberg and Castagna's relation (Castagna and Backus 1993; Greenberg and Castagna 1992). This procedure is particularly useful in generating shear sonic logs at wells where they have not been recorded. In addition, fluid properties can be estimated based on the formulas provided by Batzle and Wang (1992). The rock models are based on the Kuster-Toksoz inclusions model (Kuster and Toksoz 1974) where pores with a given aspect-ratio are mixed into a solid matrix. The propagation of seismic waves in a fluid-filled porous rock depends on rock matrix composition and structure, as well as the properties of the pore fluids. The theoretical rock models have been used to derive the effective elastic properties from rock matrix and fluid composition parameters. Model parameters are calibrated by comparison of the synthetic with the available density and compressional sonic logs. If shear sonic log data are available, then this

Table 1 Available log data in the study area in the mid Cambay Basin

Well name	P-sonic	S-sonic	Density	Remarks
A	✓		✓	Vp not reliable (not considered for the study)
B	✓		✓	
C	✓		✓	
D	✓	✓	✓	
E	✓	✓	✓	
F	✓	✓	✓	

data can also be used for calibration. The empty pores are filled with an effective fluid, assuming low sonic frequencies (Gassmann 1951). The models compose the solid matrix of two rock members. In case more than two rock members are present, the algorithms can be applied interactively to any desired level of complexity. The estimation of elastic impedance is based on two criteria. Firstly, normal-incidence reflection coefficients can be transformed directly and easily to the familiar P-wave (acoustic) impedance. Secondly, P-wave reflection coefficients are angle dependent. These criteria then lead to the concept of elastic impedance (EI) wherein angle-dependent reflection coefficients are integrated to equivalent impedances. Here, all the partial stacks and their corresponding wavelets are simultaneously inverted to P-impedance, V_p/V_s (or S-impedance) and density values. Elastic impedance inversion (EI) is a generalization of acoustic impedance for variable incidence angles. It provides a consistent and absolute framework to calibrate and invert non-zero-offset seismic data. EI allows the well data to be tied directly to the high-angle seismic data, which can then be calibrated and inverted without reference to the near offsets. EI is performed in an interactive, windows-based framework with direct access to all the required seismic, well and rock physics modelling data. It allows the user to construct as high-angle stack as is stable and then to calibrate or invert using the equivalent EI log. The elastic impedance (EI) inversion reconstructs elastic attributes, such as V_p/V_s ratio, Poisson's ratio and other attributes using angle stack AVO data (the angle stack data will be considered from seismic gather data). The following method is used to associate the three resulting reflectivity impedances with angle-dependent elastic impedance. According to Connolly (1999), EI depends on angle θ and expressed as:

$$EI = (V_p)^{1+\tan^2\theta} (V_s)^{-8K \sin^2\theta} (\rho)^{1-4K \sin^2\theta};$$

$$EI = \rho V_p (V_p)^{\tan^2\theta} (V_s)^{-8K \sin^2\theta} (\rho)^{-4K \sin^2\theta};$$

where V_p is P-wave velocity, V_s is S-wave velocity, ρ is density and K is empirically calibrated constant and equals to $(V_s/V_p)^2$. K is assumed to be constant across the reflecting boundary. However, this assumption is difficult to justify in cases of practical interest. Another serious problem with EI is that its dimensionality does not correspond to impedance and varies with θ . Variation ranges of EI with θ also strongly depend on the measurement units, and therefore it cannot be considered a constitutive property of the medium (Morozov 2010; VerWest et al. 2000).

To work around the dimensionality problem, Whitcombe (2002) proposed a normalized EI, which is the EI divided by itself measured at some reference level and scaled by AI.

$$EI = V_p \rho_o (V_p/V_po)^{1+\tan^2\theta} (V_s/V_so)^{-8K \sin^2\theta} (\rho/\rho_o)^{1-4K \sin^2\theta};$$

where V_p , V_s and ρ have been normalized by the background (average) values V_po , V_so and ρ_o . This formula is used for the elastic impedance inversion. Assuming $K = 2$, and taking the logarithm of EI and rearranging the terms, we have derived the following formula,

$$\begin{aligned} \ln(EI) - \ln(V_po \rho_o) &= \ln(V_p \rho / V_po \rho_o) \\ &+ \sin^2\theta (\ln V_p V_so / V_s V_po) \\ &- \ln V_p \rho / V_po \rho_o \end{aligned}$$

It can be seen that the logarithm of EI linearly depends on $\sin^2\theta$. Therefore, parameters of the linear trend to log-EI could be converted to V_p/V_s ratio:

$$\begin{aligned} \ln(EI) - \ln(V_po \rho_o) &= R + \sin^2\theta G; \\ V_p/V_s &= V_po/V_so \exp(G + R)/2 \end{aligned}$$

Assuming background values $V_po/V_so = 2.5$ and $\ln(V_po \rho_o) = \text{mean}(\ln EI)$.

The simultaneous inversion of synthetic gathers made from EI logs can be useful in assessing the effective resolution of the field data.

Other elastic parameters such as Lamé' parameters— μ (rigidity) and λ (incompressibility)—can be computed from the simultaneous AVO inversion. These parameters characterize the lithology and pore fluids. In this context, we define λR (LR) and μR (MR) from the inverted P and S-impedances (AI and SI; Zhou and Hilterman 2010):

$$LR = AI^2 - 2SI^2 \text{ (where AI and SI are acoustic and shear impedance)}$$

$$MR = SI^2$$

They may also be derived from P-impedance and V_p/V_s using:

$$LR = AI^2 - 2(AI^2/(V_p/V_s)^2)$$

$$MR = AI^2/(V_p/V_s)^2$$

Results

To test the resolution capabilities of the AVO inversion, synthetic gathers of P-impedance and V_p/V_s have been computed. The wavelets used in the synthetic seismogram generation and subsequent inversions were the same as those used in the inversion of the field data. The angles ranging for the synthetic gathers were also identical to the input field data. The output of log modelling describes EI (elastic impedance) for well F is shown in Fig. 3. The coloured panels in Fig. 3 show the Wavelet, Stack data

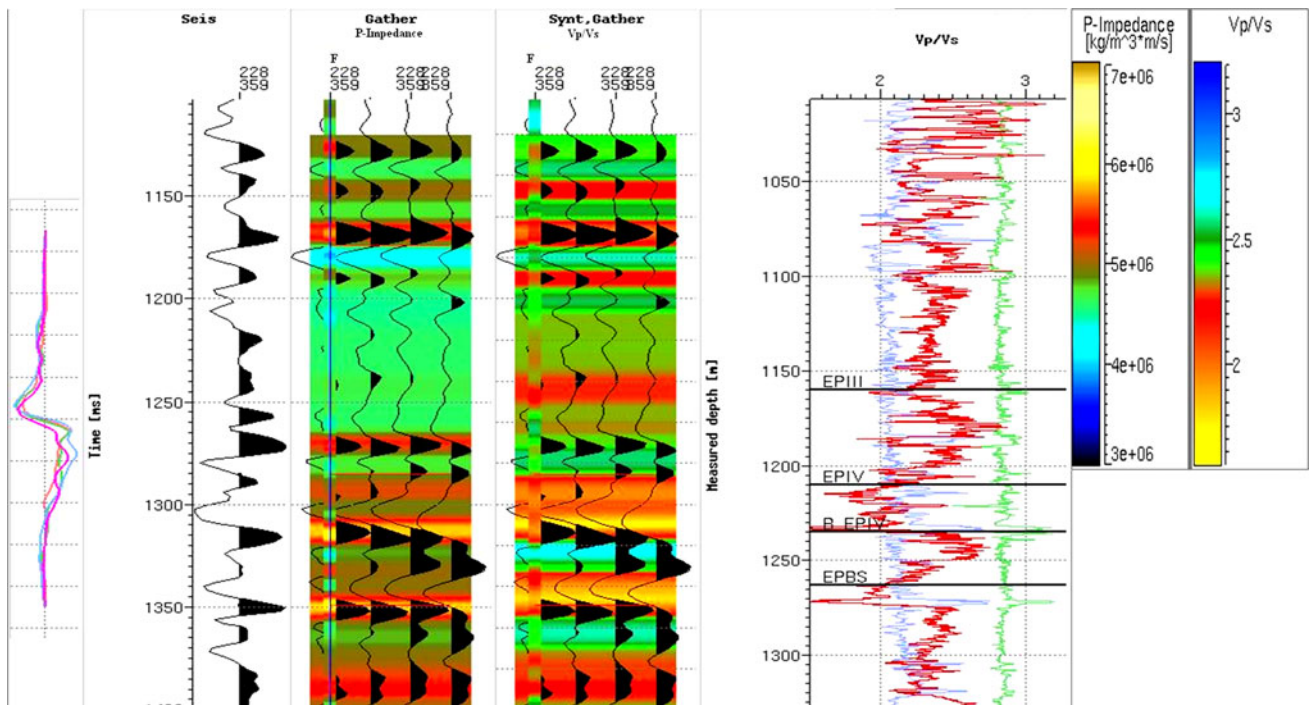


Fig. 3 The output results for elastic impedance inversion (EI) at well F. *Panel 1* Wavelets; *Panel 2* Stack 3 (26–33°) trace; *Panel 3* Synthetic angle gather with smoothed I_p log (l.h.s) over inverted

P-impedance from synthetic; *Panel 4* Synthetic angle gather with smoothed V_p/V_s (l.h.s) log over inverted V_p/V_s from synthetic; *Panel 5* *P*-sonic (blue), Density (green), V_p/V_s (red)

(26–33°), *P*-impedance and V_p/V_s from inversion with the corresponding superimposed smoothed well log. The match is generally very good and the low V_p/V_s ranging 1.4–1.5 is recovered.

Synthetic inversion data from the Eocene Pay I to Dholka Middle Pay 2 formation for a single well F is cross-plotted between *P*-impedance and V_p/V_s , in Fig. 4 colour-coded by Lambda-Rho parameter. For a final quality control (QC), the actual inversion results are compared to the well log data in Fig. 5. It is observed that the correlation between the inversion results from synthetic seismogram and inversion results from actual seismic data is good.

Geological modelling

Geologic modelling is used to add a consistent low-frequency component to the inversion, thus placing the high-frequency information from the seismic reflection data into a reasonable geologic setting. The structure of the 3D geologic model is defined by two pieces of information—the interpreted horizons and the model ‘framework’. The framework, in the form of a spreadsheet, describes the ordering of the horizons in space and time and their behaviour at faults. The horizons, which can include interpreted faults, provide structure information. Together, these form a ‘blueprint’ for the model. Stratigraphy within

the layers is specified as onlap, offlap, reef, channel, etc. The model is completed by populating it with geophysical information, usually in the form of well logs. The logs are most commonly provided in depth and the horizons in time. It is therefore necessary to create a time-depth transformation if these two pieces of information are to be rationalized. Input sonic logs are integrated, hung on an input time datum and drift-corrected to tie the time horizons. Since sonic log is showing different nature in gas-bearing and oil-bearing reservoir pay sand in this study area, this correction is required. This then provides the logs in time to enable the model to be built.

Results

Seismic processing velocity (in form of RMS) has been converted to seismic interval velocity using Dix conversions. In this study area, the seismic interval velocities have been combined with well log velocities in the deeper section and calibrated back to the well logs. This volume was then converted to *P*-impedance and combined with the higher frequencies in the well logs to create a model of *P*-impedance that also contains information from the seismic velocities. As seismic velocities only contain very low-frequency information (2–3 Hz at maximum), these have been merged in with higher frequencies from the well data.

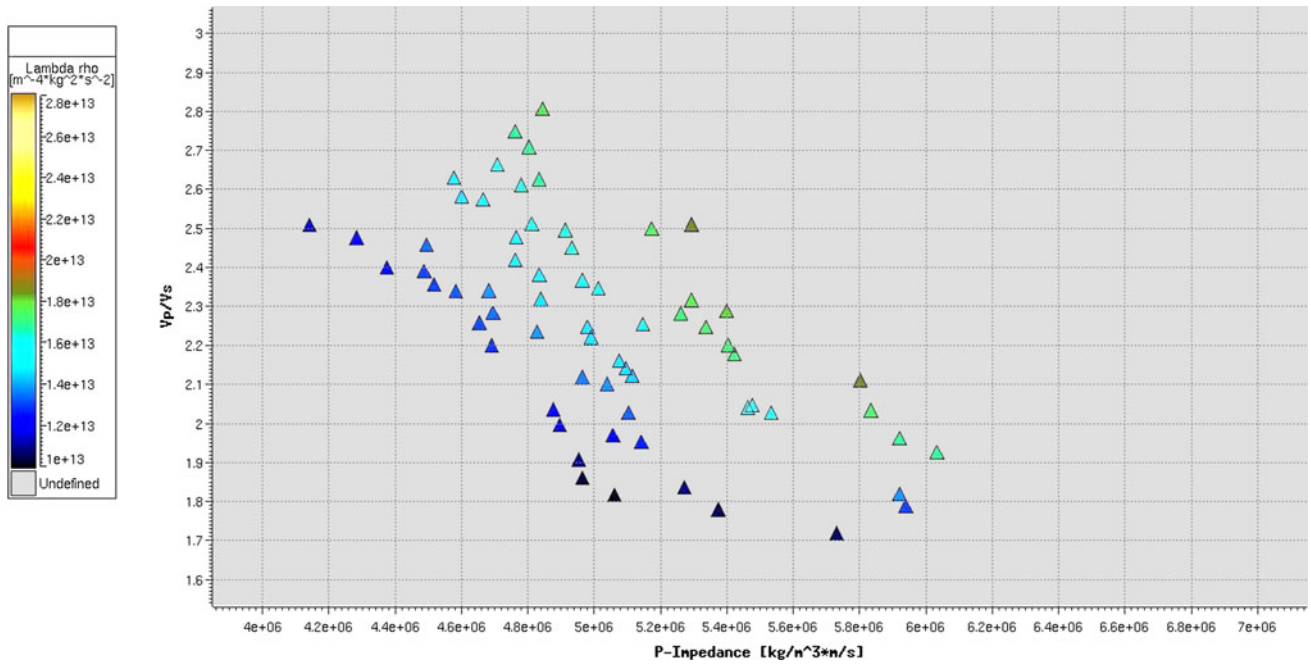


Fig. 4 P-Impedance versus Vp/Vs cross-plot coloured by Lamda * Rho using well data in vertical gate 1,100–1,420 ms (Eocene Pay I to Dholka Middle Pay 2) to distinguish the reservoir and non-reservoir part

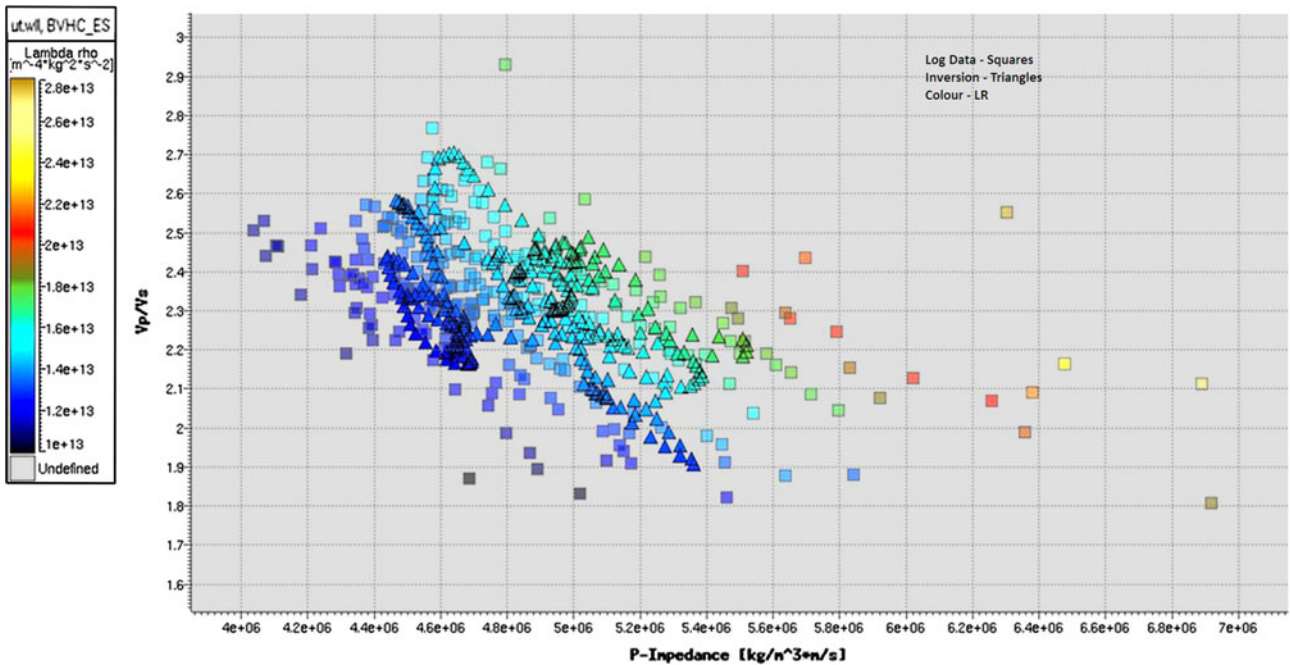


Fig. 5 P-impedance versus Vp/Vs cross-plot coloured by Lamda * Rho using Well data and extracted pseudo well log data from inverted volume at the well location in the vertical gate

1,100–1,420 ms (Eocene Pay I to Dholka Middle Pay 2) to distinguish the reservoir and non-reservoir part along with QC of the inverted P-impedance and P-impedance at well level

Wavelet analysis

Wavelet analysis is conducted by computing a filter that best shapes the well log reflection coefficients to the input

seismic at the well locations. The phase of the seismic data, which may vary with frequency, is found from the inverse of this filter. During the analysis procedure, separate estimates are made of the spectra of the input seismic

reflection data, the reflection coefficients implied by the well logs and the seismic wavelet. The wavelet is further fine tuned by testing its efficacy in performing constrained sparse spike inversion on traces near the well. This wavelet, with amplitude representative of the seismic, is input directly to the inversion algorithm or used to explicitly correct the seismic phase to zero. If the latter route is chosen, then an equivalent zero phase wavelet must be input to the inversion.

In AVO inversion, wavelets corresponding to each of the input offset or angle-limited stacks are needed. They are derived by first computing elastic impedance (EI) logs (and hence reflection coefficients) from the P and S sonic and density logs at the angle ranges corresponding to the partial stacks. From the matching of the limited stack data to these EI logs, the wavelets for each stack are found. This procedure ensures that offset-dependent phase and amplitude effects are correctly taken into account.

Results

Due to the nature of the seismic data, three different vertical windows have been used for estimating wavelets and running the inversions. This is because there is a large drop in frequency content and amplitude with increasing time; for an optimum inversion result, different wavelets need to be used. The final results were merged together laterally and vertically. The different vertical gates have been set around time horizons. These are as follows:

- Shallow Window 1: Miocene Basal Sand – 300 ms to Eocene Pay I + 50 ms
- Mid Window 2: Eocene Pay I – 50 ms to Dholka Middle Pay 2 + 120 ms
- Deep Window 3: Dholka Middle Pay 2 + 100 ms to Deccan Trap + 800 ms

The wavelet estimation time windows were defined by time horizons picked individually around each of the three wells (D, E and F). In the final inversions, it was decided that stack 9 (33–46) should not be used as the wavelet was dramatically different from all other stacks, making it difficult to obtain a consistent seismic to well tie.

Although the agreement is generally good, there is some degradation in the furthest stacks. The final wavelets for inversion and their spectra are plotted together. They were obtained from a multi-well amplitude variation with angle (AVA) wavelet estimation process using wells D, E and F. There is a clear degradation in high-frequency power at increasing angles. The phase is around -90° , but slightly variable with frequency.

Figure 6 is an example of several QC spectra for well D. The Fig. 6 is indicating the spectra for the wavelet, seismic, inversion reflectivity, well reflectivity and residual.

The residuals are low and the inversion spectrum is very similar to the log spectrum over the seismic band. Also shown are the estimated wavelets for the shallow section, from each well. They are very similar to each other, indicating that the seismic data are consistent across the survey.

Data alignment

To achieving an accurate inversion correct time alignment of the input partial stacks is must required. The wavelets encode within themselves bulk shifts, since adjustment of the input well logs (shifting, stretching, squeezing) is only allowed once for the reference stack. However, other time-dependent residual normal moveout (NMO) effects can exist between the wells. These can be addressed by applying alignment corrections to the input stacks. The corrections may be computed from correlation techniques designed from the input stacks or their individual inversions, or from interpretations of events on the individual inversions. V_p/V_s , which are a direct output of the simultaneous inversion, are a key alignment QC diagnostic. When misaligned stacks are subjected to inversion, anomalously high or low values of V_p/V_s can develop. V_p/V_s can, in fact, be driven below its theoretical lower limit of 1.414. Mapping of these anomalous regions can highlight areas of misalignment.

Results

These seismic stacks appear to be well aligned and, due to the presence of significant noise, any attempt to improve this may not provide an optimum solution. Figure 7 shows a comparison of one input stack (33–40°, black wiggles) with its synthetics from a simultaneous inversion run (blue wiggles). These show a very good agreement, given the presence of noise in the data; due to the nature of the inversion algorithm, any misalignment in between the stacks will show up in the inversion synthetics.

Simultaneous inversion quality control

The input seismic data are modelled by the convolution of the seismic wavelet with the inverted reflection coefficient series. Because the seismic wavelet is band-limited, the problem is non-unique. There are many reflection coefficient series that, when convolved with the seismic wavelet, reproduce the input seismic to arbitrary accuracy. The post-stack seismic resolution inversion technique is the constrained sparse-spike inversion (CSSI). This assumes a limited number of reflection coefficients, with larger amplitude. The inversion results in acoustic impedance (AI), which is the product of rock density and p-wave

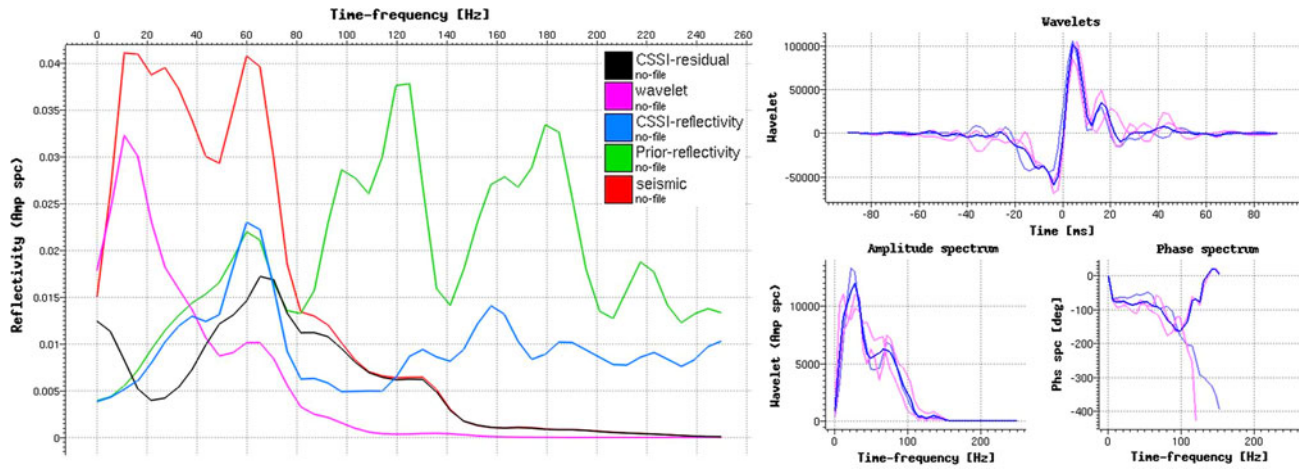


Fig. 6 Final estimated wavelet QC along with phase spectrum and amplitude spectrum

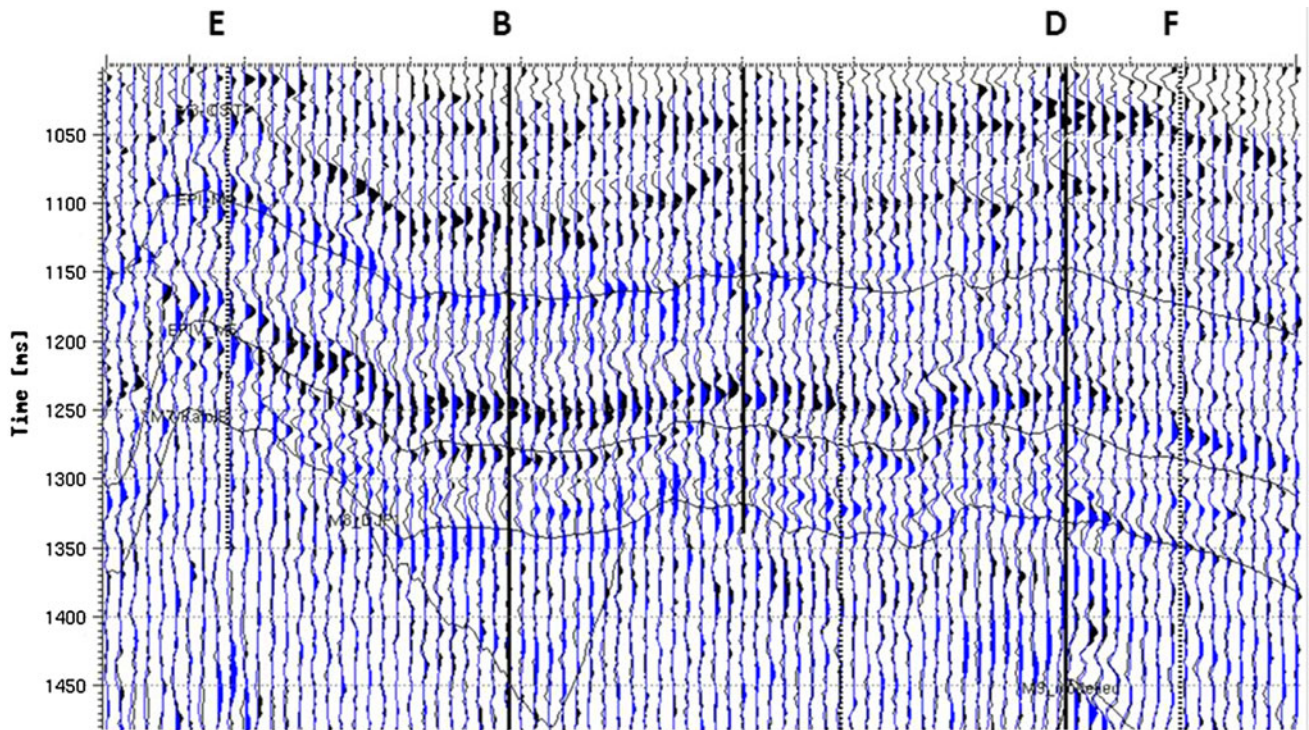


Fig. 7 Data alignment QC; Black seismic data, Blue synthetic data from simultaneous inversion

velocity. Unlike seismic reflection data (which is an interface property), AI is a rock property. The model generated is of higher quality and does not suffer from tuning and interference caused by the wavelet. The benefits of this special type of inversion CSSI over the other inversion techniques have been mentioned below.

Inverted seismic data describe the layer property of the subsurface and much more informative, which can give information about the facies change of reservoir. Through this information, we can reach near to the truth that helps us in exploration business. Inversion of seismic data to

impedance improves exploration and reservoir management success, producing more hydrocarbons with fewer, more highly productive wells. Among the improvements are:

- Higher resolution through reduction in the wavelet effects, tuning and side lobes.
- Incorporation of low frequencies not contained in the seismic data.
- Increase asset team interaction through the use of layer-based (versus interface) acoustic impedance models that are readily understood by all asset team members.

- Accurate rock property modelling, as impedance can be related to several key rock/ petrophysical properties such as porosity, lithology and water saturation.
- Better understanding of the accuracy of seismic processing and acquisition, well log data and quality, and quality of input interpretations. Through rigorous tying of the wells to the seismic and estimation of the waveform that is in the earth and the seismic inversion of the data back to well control, the asset team can better understand accuracy and consistency of the input data.

CSSI transforms seismic data to a pseudo-acoustic impedance log at every trace. Acoustic impedance is used to produce more accurate and detailed structural and stratigraphic interpretations than can be obtained from seismic (or seismic attribute) interpretation. In many geological environments, acoustic impedance has a strong relationship to petrophysical properties such as porosity, lithology and fluid saturation.

A good (CSSI) algorithm will produce four high-quality acoustic impedance volumes from full or post-stack seismic data: full-bandwidth impedance, band-limited impedance, reflectivity model and low-frequency component. Each of these components can be inspected for its contribution to the solution and to check the results for quality. To further adapt the algorithm mathematics to the behaviour of real rocks in the subsurface, some CSSI algorithms use a mixed-norm approach and allow a weighting factor between minimizing the sparsity of the solution and minimizing the misfit of the residual traces. Thus, agreement of the sparse spike synthetic with the seismic becomes a necessary but not a sufficient condition in the solution of the inversion problem. An important constraint is the relative importance placed on minimizing either the mean square model error or the magnitude of the estimated reflection coefficients. This weighting factor called the ‘Lambda Parameter’ controls the trade-off between sparsity or blockiness and the fit of the generated acoustic impedance trace to the seismic data. Knowledge of the expected trace-to-trace impedance variations can also be provided to limit the solution space as required. Since there is no guarantee in the mathematics that there will be agreement between the computed inversion and the impedance logs, quality control can be done by comparing them.

Although the constraints in sparse spike inversion will guarantee the existence of low frequencies in the inversion, we do not expect that the information in the lowest frequencies will be reliable. This is a consequence of the band-limited nature of the seismic wavelet. The lowest reliable frequency will be project dependent, depending upon the quality of the input seismic and the constraints

applied to it. The frequencies in the constrained sparse spike inversion just below the input seismic bandwidth are driven by the impedance constraint fairway. In the final inversion, these frequencies can be drawn from the seismic or model as appropriate. At some lower (merge) frequency, the information should come from the model. The model can be computed using logs from a single well or many, depending upon the circumstances. The former option will guarantee that no lateral varying information beyond that due to structure can come from the model while the latter will include the most available information about the project area. In addition to outputting the final merged inversion, a seismic-only version is also produced, which contains no model contribution at all. Since this inversion contains no low frequencies, it is referred to as a relative inversion. The merged output is referred to as the absolute inversion.

Results

The low-frequency trends (filtered back to 20 Hz) for P-impedance, density and Vp/Vs for wells D, E and F were used to softly constrain frequencies below the seismic band. Quality control of the inversion was done for a few traces around each of the wells. Then, the algorithm norm setting was chosen to produce the most reliable, low variance result. To choose an appropriate norm control, the algorithm was run for a series of values on three traces around the key wells. The rate of change of S/N with the value of the Lambda parameter is at first sharply increasing, then flat. This behaviour is characteristic of an efficient and accurate wavelet. The values of the S/N are consistently between 4 and 5 dB for all stacks. After several simultaneous inversion tests at the wells, a value of 17 was chosen for the final inversion for this time window (mid). For the shallow and deep inversion windows, a Lambda value of two was sufficient.

Simultaneous AVO inversion—fluid characteristics through P-impedance and S-impedance

Simultaneous elastic inversion of angle or offset-limited stacks provides quantitative AVO information. Since unique wavelets are estimated for each stack, compensation is automatically done for the effects of tuning, scaling and NMO stretch—all of which can be offset dependent. The simultaneous inversion produces volumes of P-impedance, Vp/Vs (or S-impedance) and density. This in turn can be used to compute other parameters of interest such as the Lamé parameters: Lambda and Mu. Density is usually ill defined for the range of AVO and acquisition situations commonly encountered. In these cases, it can be set to be

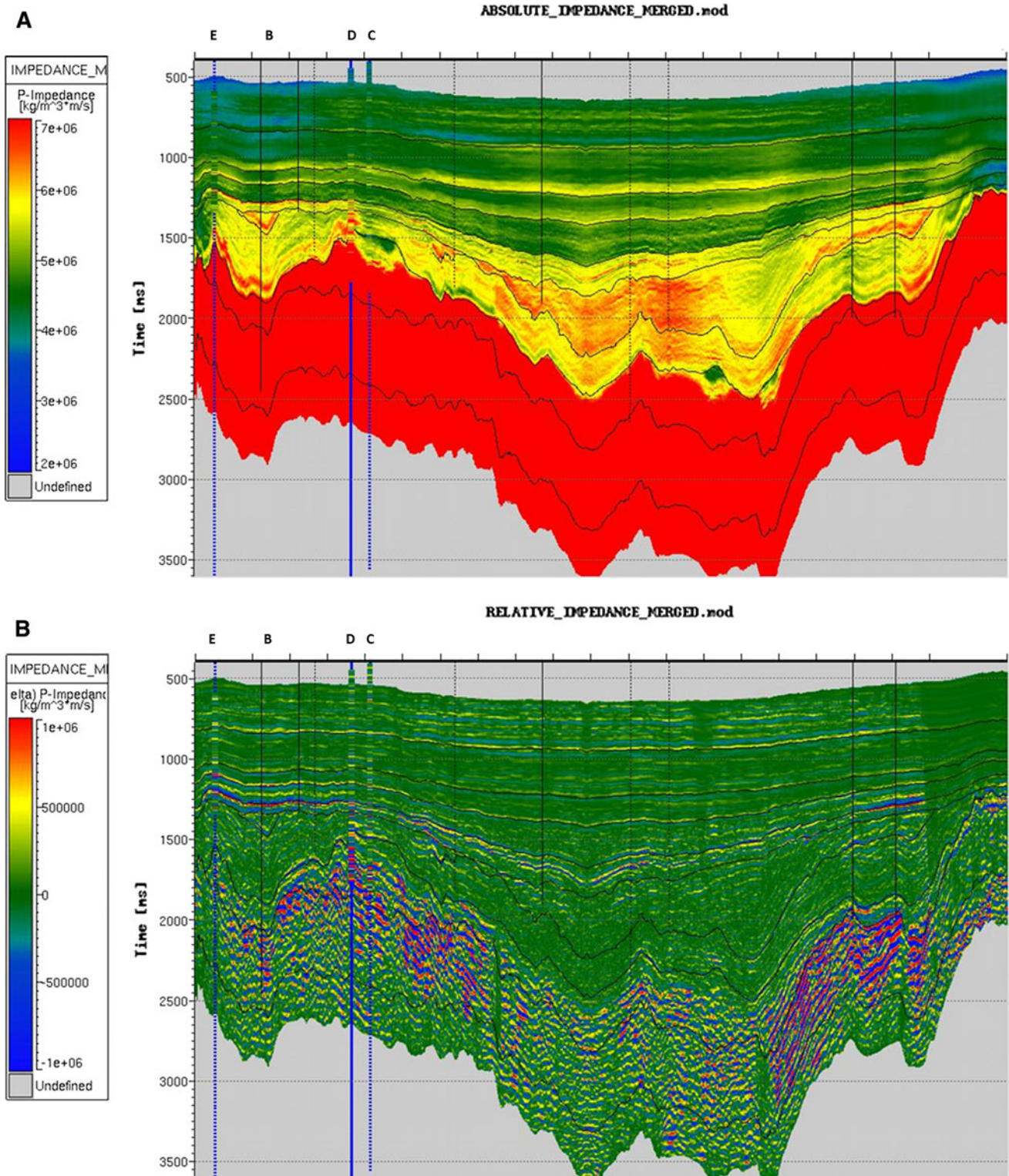


Fig. 8 Fluid characterization through absolute and relative P-inversion study

constrained closely to the P-Impedance solution via Gardner's relation (Gardner et al. 1974).

The algorithm works by first estimating zero-offset P-wave reflection coefficients. These are extended to angle-

dependent impedances, $P(\theta)$, using the observed offset information from the stacks. Next, the Zoeppritz equations (1919) are used to make initial seismic-band estimates of the elastic reflection coefficients for P, S and density. These

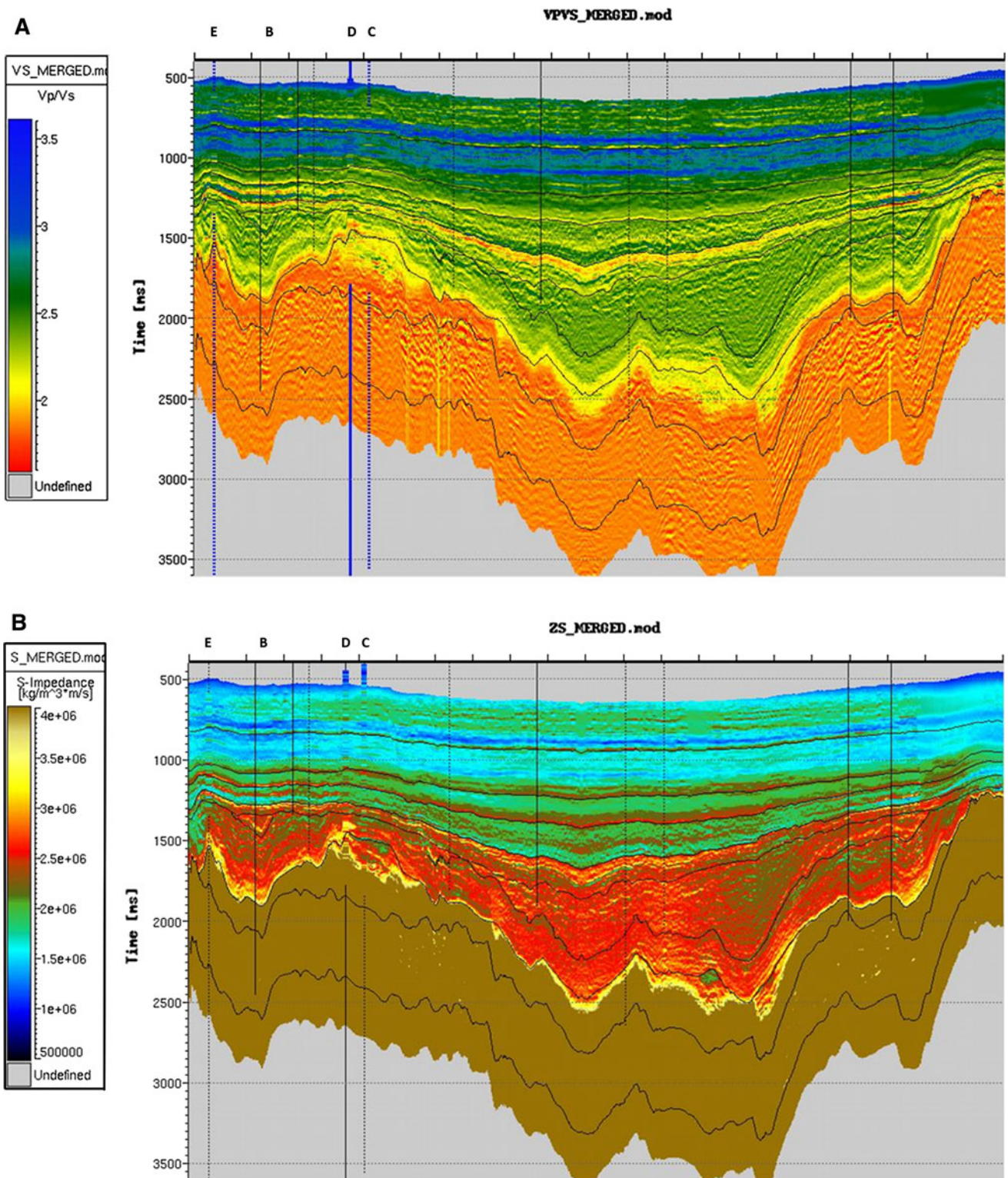


Fig. 9 Fluid characterization through Vp/Vs inversion and shear impedance study

are then merged with their low-frequency components from the model and integrated to produce broadband P and S-impedances and density. In the last step, hard and soft constraints sets are applied and the solution reworked.

Results For the average signal-to-noise ratio (S/N) at each Common Mid Point (CMP) after inversion for the reference, stack three values are generally between 2 and 5 across the study area with some patches of degradation.

Figure 8a and b illustrates the absolute and relative acoustic impedance and Fig. 9a and b displays the outputs from inversion study of V_p/V_s inversion and shear impedance. To achieve the V_p/V_s inversion, the low-frequency component (below the seismic bandwidth) has been included. The low-frequency component of P-impedance or V_p/V_s will be affected by lithology and fluid saturation. In this study, we have used relative property of band-limited P-impedance and V_p/V_s to identify the reservoir pay sand (Hughes et al. 2008) and then merged into the low-frequency model. The benefit of this approach is that the distributions of the reservoir pay sand in the final low-frequency model are data driven rather than model driven. The log data indicate that the sandstones in this study area exhibit high impedance and expected low V_p/V_s and serve as a good quality check on the inversion mechanism. On the shear impedance volume through lithology log, reservoir containing different pore fluids like oil sand, water sand and brine sand have been identified at well location as well as away from the well location.

Time-to-depth conversion and pseudo-log extraction

Depth conversion consists of two parts. The first is the establishment of a datum that exists in both time and depth and represents the same geologic horizon. Normally, a clear time horizon not far from the region of interest is chosen. The method works best when there are several

depth tops at the datum available. Then, an interpolation function can be designed to interpret datum values between the wells at every CMP (Domenico 1976).

In the second phase, an interval velocity function is used to convert regions away from the datum to depth. The velocity function can come from the geologic model or a scaled version of the inversion. The depth conversion is checked by comparing other depth-converted horizons to their corresponding depth tops at the wells.

Results

The final data volumes have been converted to depth, using the calibrated seismic velocity cube; this is a straightforward procedure. The datum was set to MSL in TVD and 0 ms in TWT for this process. A first-pass time-to-depth conversion was compared to the well markers in depth and a residual correction applied to the velocity cube to optimize the tie. This residual correction was less than 3%. The final, adjusted velocity cube is shown in Fig. 10. To illustrate the match with the well data in depth, the V_p/V_s data in TVD is correlated with the original well logs data. The match is very good at the three wells.

As a final QC on the well data versus the inversion, pseudo-logs have been extracted from each of the depth-converted derived cubes, in particular P-impedance and V_p/V_s . These extracted logs are cross-plotted, at seismic sampling, against the actual log data in Fig. 11 (P-impedance)

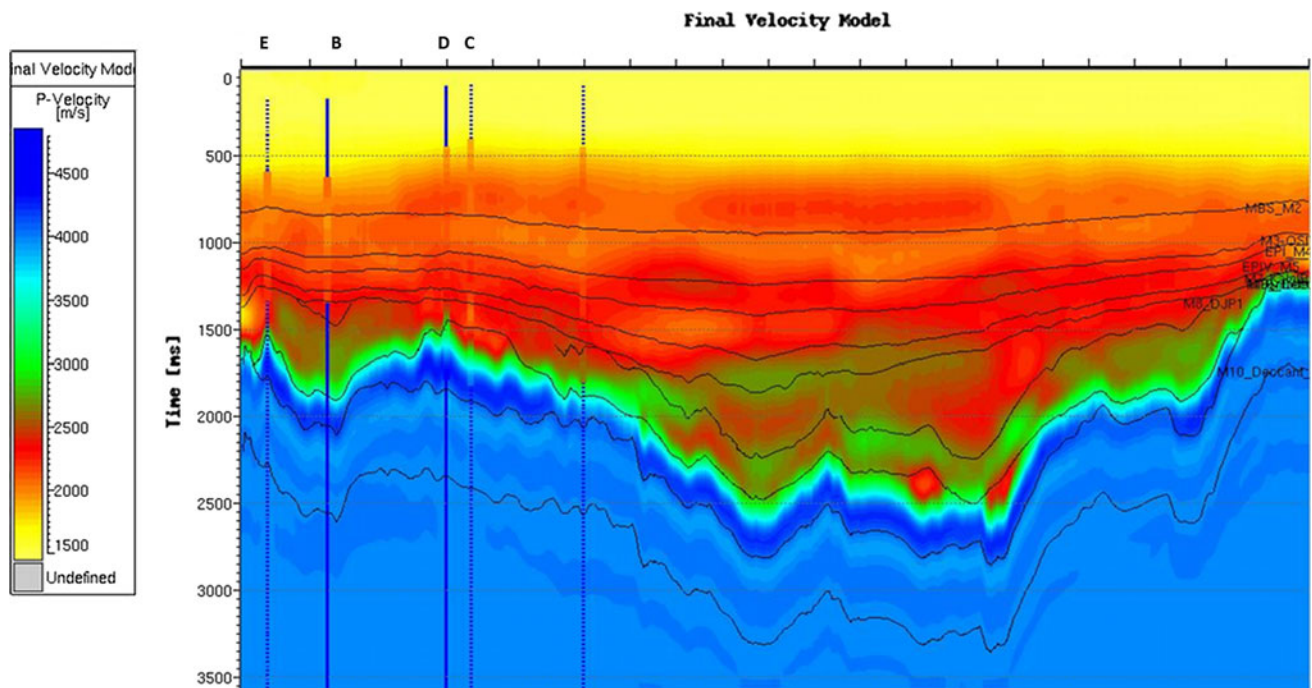


Fig. 10 Final velocity cube for time-to-depth conversion

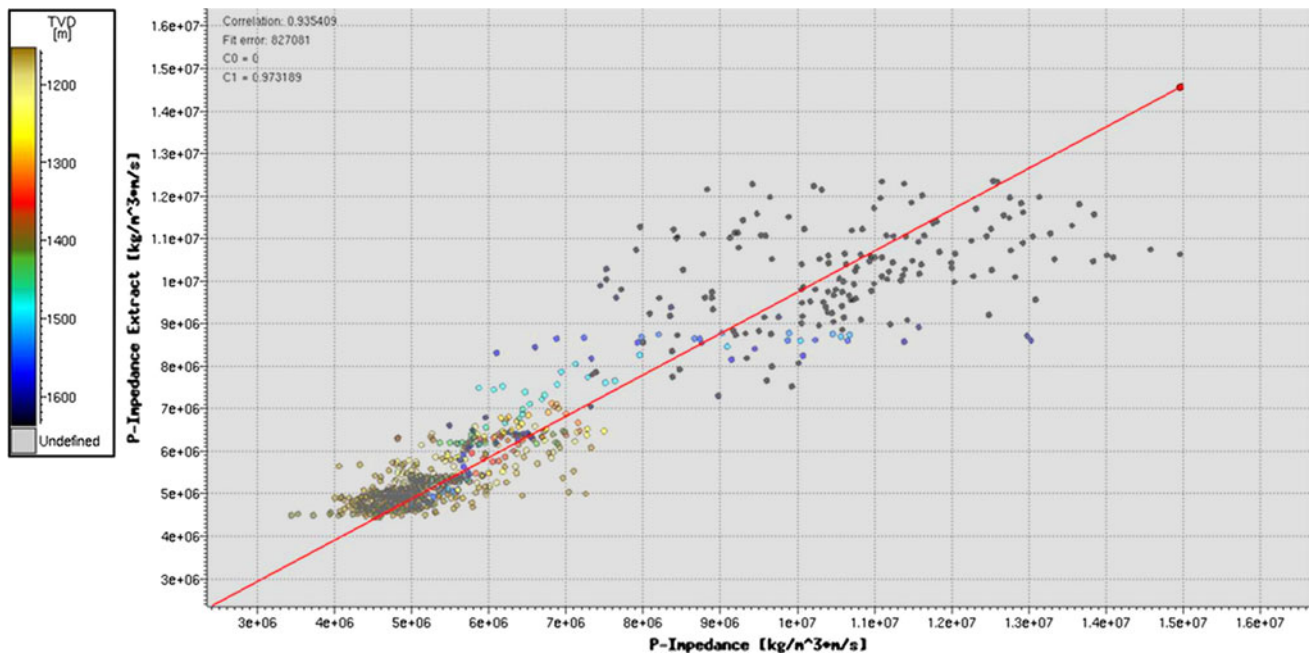


Fig. 11 Well log derived P-impedance versus extracted P-impedance for depth matching QC

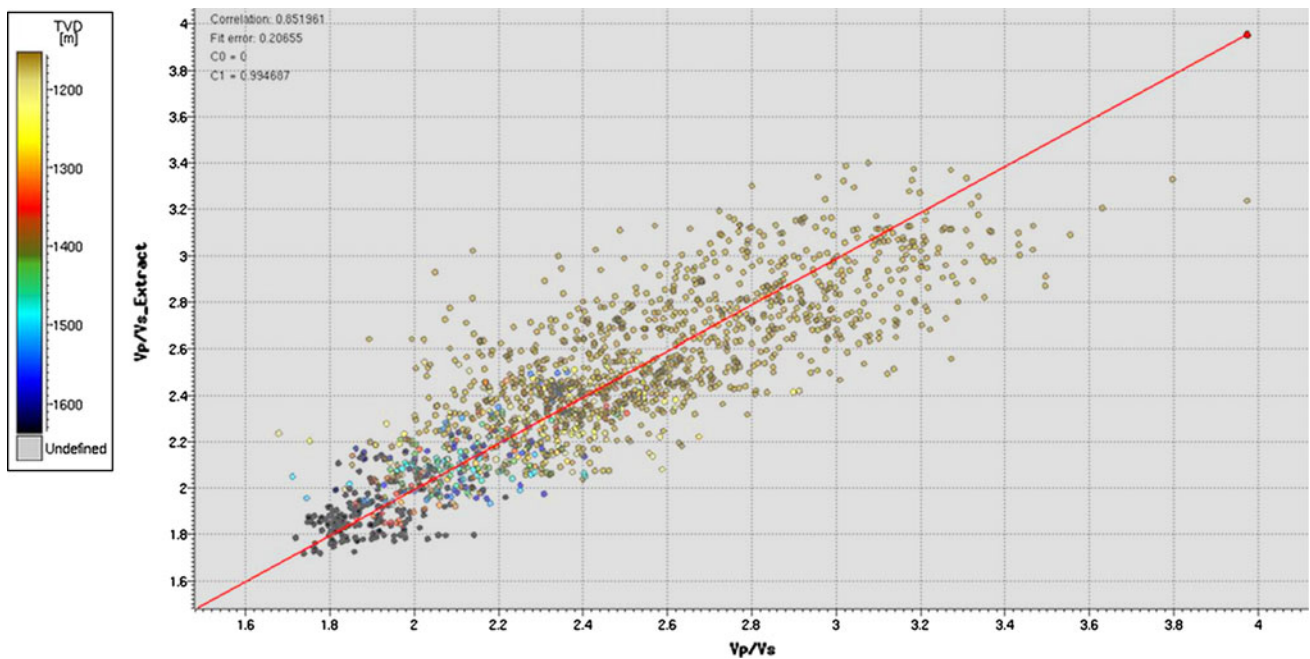


Fig. 12 Well log derived Vp/Vs versus extracted Vp/Vs for depth matching QC

and Fig. 12 (Vp/Vs). It may be observed from the Figs. 11 and 12 that a very good correlation exists between actual logs derived and inverted data. This further indicates that depth conversion process is also working correctly. For the whole log interval, from Miocene Basal Sand (MBS) to Deccan Trap, a cross-plot of Vp/Vs against P-impedance is shown in Fig. 13. The data points are overlain with colours indicating

the bulk volume of hydrocarbon (hydrocarbon pore volume), which has been calculated through petrophysical property.

$$\begin{aligned} \text{Hydrocarbon pore volume} &= \text{GRV}(\text{gross rock volume}) \\ &\quad * \text{net to gross ratio} \\ &\quad * \text{porosity} \\ &\quad * \text{hydrocarbon saturation.} \end{aligned}$$

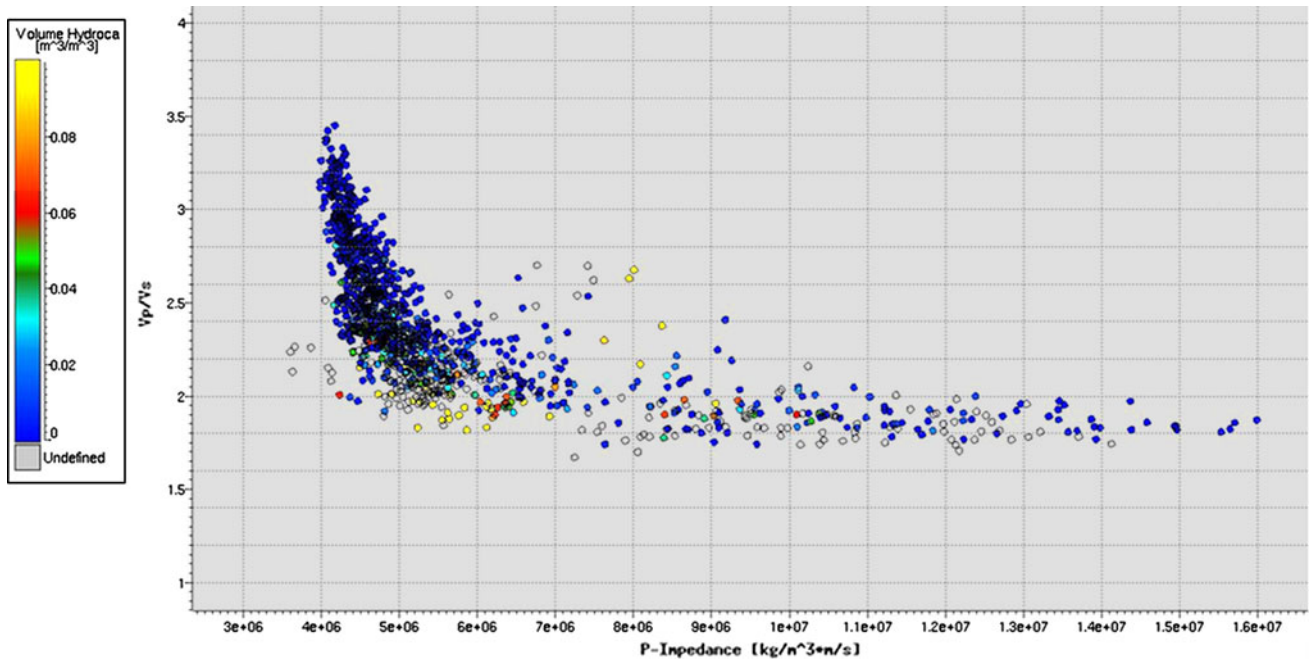


Fig. 13 P-impedance versus Vp/Vs coloured with bulk volume hydrocarbon

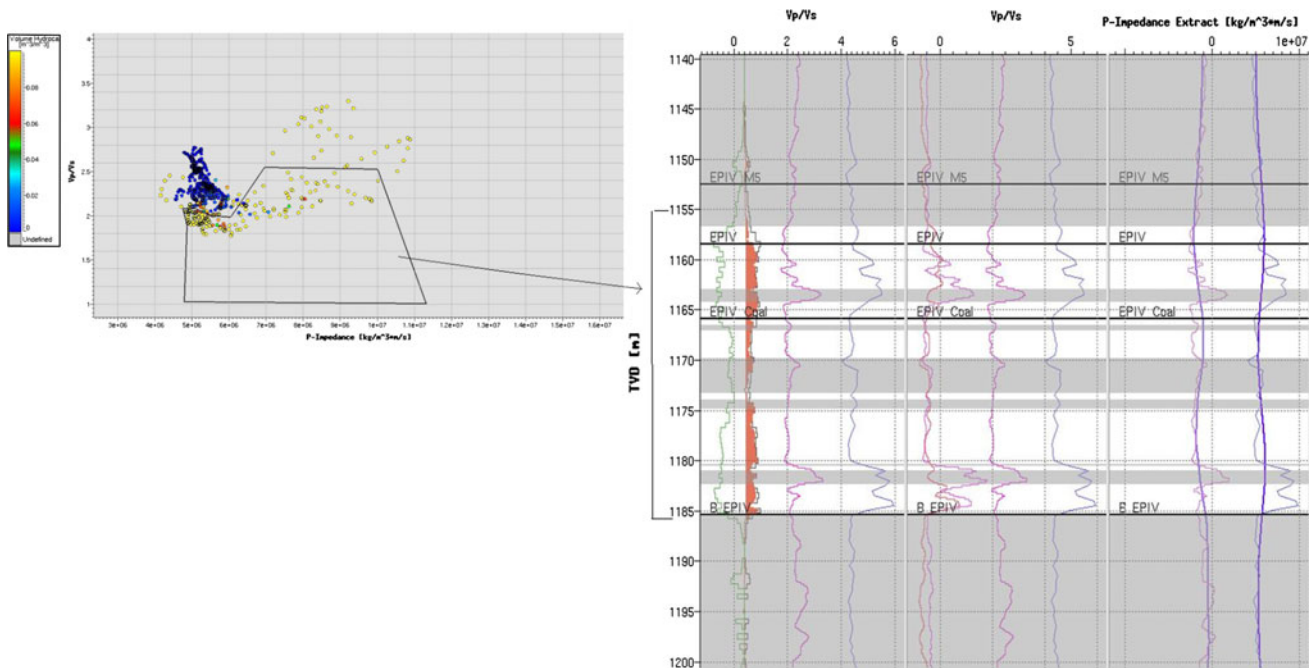


Fig. 14 Highlighting pay with Vp/Vs and P-impedance at Eocene IV level; after capturing promising data points in the cross-plot, the interested pay zone at well profile has been directly highlighted

The above petrophysical data point has been extracted from inverted volume (P-impedance and Vp/Vs).

Identification of prospective pay zones

The data points are coloured with bulk volume of hydrocarbon, and the contribution from different layers is

indicated (Wijngaarden et al. 2004). This plot further refined in Fig. 14 is displaying the data points from a layer bounded by the depth surfaces Eocene Pay IV and Kalol Base, sampled at 4 m in true vertical depth (TVD). The polygon highlights the hydrocarbon-bearing sands, which exhibit lower Vp/Vs and relatively high P-impedance. The highlighted section is shown in the log

panel on the right and covers the main reservoirs in Eocene Pay IV. To capture the reservoir pay sand, another rock physics template, namely cross-plot of $\text{Lambda} * \text{Rho}$ vs $\text{Mu} * \text{Rho}$, was made (Fig. 15) and 3rd axis is considered as different lithology column of Cambay Shale; the closed polygon captured the reservoir sand through the anomalous cluster data points. The

same is also synchronized with the well log panel. Stratigraphic slices have been constructed in the layer bounded by the Eocene Pay IV and Kalol Base horizons, in depth; internal stratigraphy is being defined to be conformable to top and base. The sands are observed as areas of lower V_p/V_s and have clear features of indicating sand development against palaeofaults. The faults

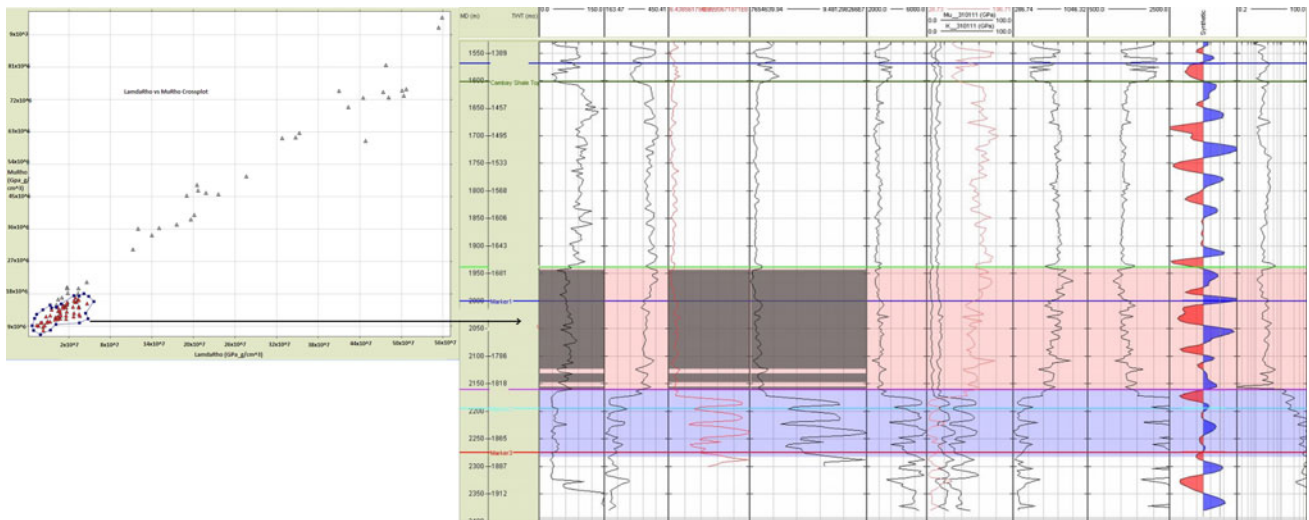


Fig. 15 $\text{Lambda} * \text{Rho}$ versus $\text{Mu} * \text{Rho}$ Cross-plot. Closed polygon at Lower Cambay shale along with well log panel from well E—3rd axis considered as zone (Cambay shale)

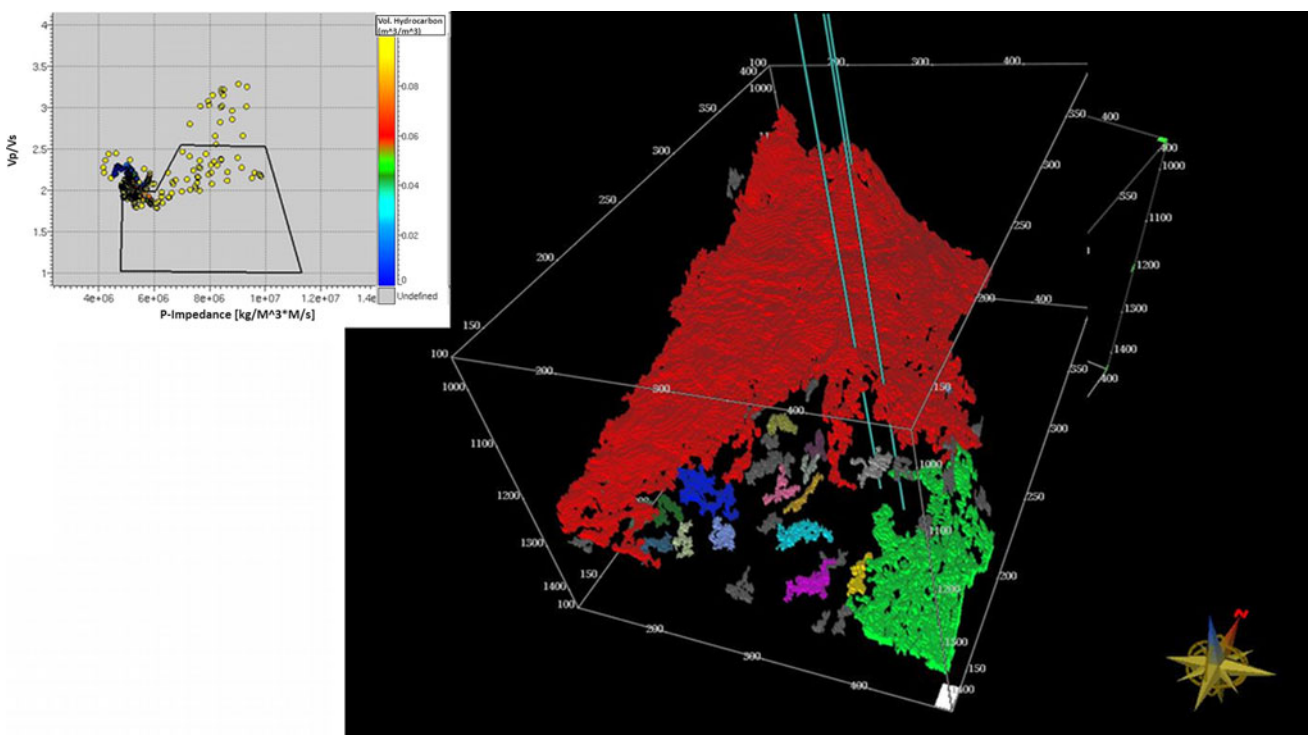


Fig. 16 Body-checking of reservoir pay sand based on P-impedance and V_p/V_s

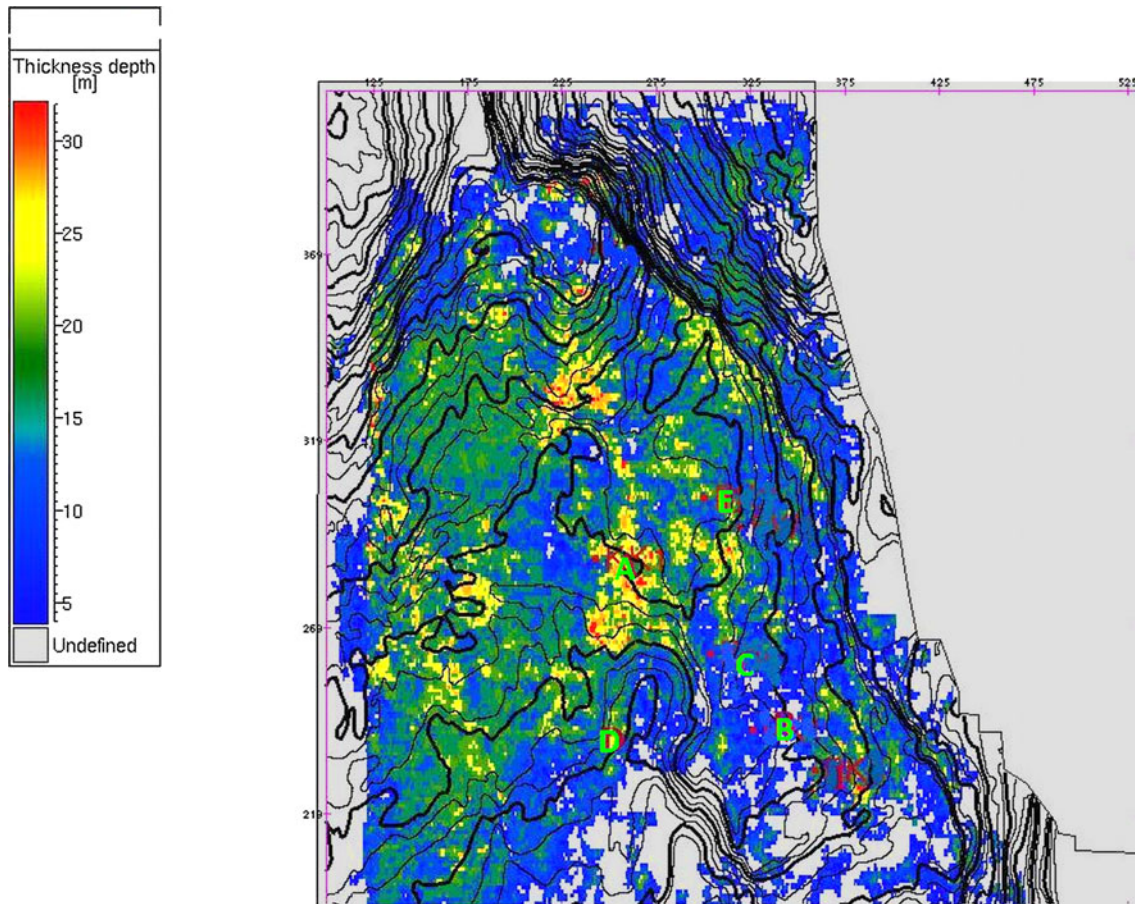


Fig. 17 Thickness of reservoir pay sand of captured bodies

at this level do not penetrate to surface. Visible regions in the plots have been generated from probable sands. By applying the same area, geobodies corresponding to possible hydrocarbon-bearing sands are captured (Fig. 16). Figure 17 shows the thickness of these captured sand bodies in map view, overlain with contours of the Eocene Pay IV surface in depth.

Conclusions

Elastic impedance inversion provides a consistent and absolute framework to calibrate and invert non-zero-offset seismic data. EI allows the well data to be tied directly to the high-angle seismic data, which can then be calibrated and inverted without reference to the near offsets. In this work, the output of ‘Log modelling’ for well E has indicated low V_p/V_s ranging 1.4–1.5 in reservoir and non-reservoir section. Simultaneous AVO inversion has been used to successfully compute P-impedance and V_p/V_s volumes from the input partial-angle stacks. These were

then used to estimate S-impedance, $\Lambda\rho$ and $\mu\rho$. Agreement with well control was generally good for P-impedance and V_p/V_s as displayed in Figs. 11 and 12. In the study area, hydrocarbon prospective zone has been marked through compressional (P wave) and shear wave (S wave) impedance only. In the RPT analysis, we have plotted different kinds of graphical responses of Lamé’s parameters, which are the function of P-wave velocity, S-wave velocity and density. The discrete thin sand reservoirs have been delineated through the RPT analysis. Based on the inversion result and RPT analysis, the prospective area along with reservoir sand is defined as described in Fig. 18. Attribute extraction and 3D visualization also show the sand development against palaeofaults and may also indicate the presence of hydrocarbon fill. Through this fluid characterization, oil-bearing thin sand layers have been found in well E including well D.

In recent time, it is a difficult job to explore the reservoir sand in this area since most of the area has been explored. The reservoir quality of the rest unexplored field in Cambay Basin is not so good, and in this situation, this kind of

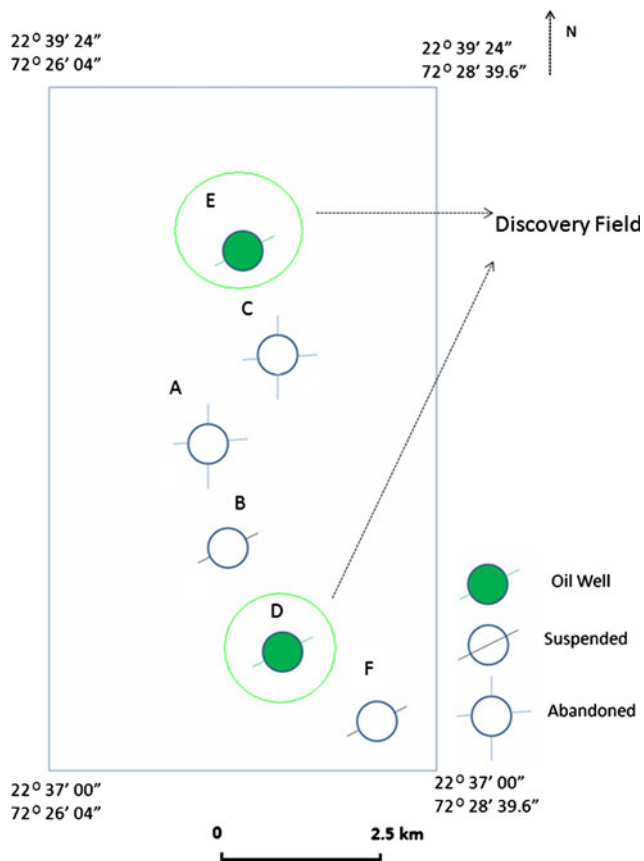


Fig. 18 The study area along with oil discovery field after the study

inversion and rock physics study will help the exploration world to explore thin and discrete reservoir sand of tight formation in the Cambay Basin.

Acknowledgments We gratefully acknowledge the Gujarat State Petroleum Corporation Limited, Gandhinagar, Gujarat, regarding the various data support and analysis in this area of the Cambay Basin. We are also acknowledging the Fugro Jason and M/s Schlumberger personnel for their extensive and close study in inversion and well log study of this area. Our sincere gratitude to the Ikon Science for using RokDoc application for rock physics study and Fugro Jason for using JGW application for inversion study.

References

- Avseth P (2000) Combining rock physics and sedimentology for seismic reservoir characterization of North Sea turbidite systems, Unpublished PhD thesis, Stanford University
- Avseth P, Mukerji T, Mavko G (2005) Quantitative seismic interpretation: applying rock physics to reduce interpretation risk. Cambridge University Press, Cambridge
- Balakrishnan TS, Gupta TC, Bisht HS (1977) Regional tectonic and sedimentation studies of Cambay Basin: unpublished report, ONGC
- Banerjee A, Pahari S, Jha M, Sinha AK, Jain AK, Kumar N, Thomas NJ, Misra KN, Chandra K (2002) The effective source rocks in the Cambay Basin, India. AAPG Bull 86(3):433–456

- Batzle M, Wang Z (1992) Seismic properties of pore fluids. Geophysics 42:1369–1383
- Brie A, Pampuri F, Marsala AF, Meazza O (1995) Shear sonic interpretation in gas bearing sands. Society of Petroleum Engineers, Paper id 30595
- Castagna JP, Backus MM (1993) AVO analysis-tutorial and review. In: Castagna J, Backus MM (eds) Offset-dependent reflectivity. Theory and practice of AVO analysis, vol 8. SEG, pp 3–37
- Chi X, Han D (2009) Lithology and fluid differentiation using rock physics templates. Lead Edge 28:60–65
- Connolly P (1999) Elastic impedance. Lead Edge 18:438–452
- Davies MR, Portniaguine O (2004) Elastic attribute generation from 3 points elastic inversion, OTC 16731, Offshore Technology Conference, Houston, Texas, USA
- Domenico SN (1976) Effect of brine-gas mixture on velocity in an unconsolidated sand reservoir. Geophysics 41:882–894
- Dvorkin J, Nur A (1996) Elasticity of high porosity sandstones: theory of two North Sea data sets. Geophysics 61:1363–1370
- Fatti JL, Smith GC, Vail PG et al (1994) Detection of gas in sandstone reservoirs using AVO analysis: a 3-D seismic case study using the Geostack technique. Geophysics 59:1362–1376
- Gardner GHF, Gardner LW, Gregory AR (1974) Formation velocity and density—the diagnostic basis for stratigraphic traps. Geophysics 39:770–780
- Gassmann F (1951) Elastic waves through a packing of spheres. Geophysics 16:673–685
- Gray D, Goodway W, Chen T (1999) Bridging the gap: using AVO to detect changes in fundamental elastic constants: 69th Ann Internat Mtg, Soc Expl Geophys, Expanded Abstracts, pp 852–855
- Greenberg ML, Castagna JP (1992) Shearwave velocity estimation in porous rocks: theoretical formation, preliminary verification and applications. Geophys Prospect 40:195–210
- He FB, You J, Chen KY (2011) Gas sand distribution prediction by elastic inversion based on rock physics modelling and analysis. Appl Geophys 8(3):197–205
- <http://www.fugro-jason.com/software/powerlog/RPM.htm>, July 2011, 14:00 pm (approx.)
- http://en.wikipedia.org/wiki/Seismic_inversion, July 2011, 16:00 pm (approx.)
- Hughes P, van Eykenhof R, Mesdag P (2008) Estimation of Hydrocarbons in-place by simultaneous (AVO) inversion, constrained by iteratively derived low frequency models, Fugro-Jason AS, PO Box 8034, 4068, Stavanger, Norway
- Kundu J, Wani MR (1992) Structural style and tectono-stratigraphic framework of Cambay rift basin, Western India. Indian J Petroleum Geol 1(2):181–202
- Kuster G, Toksoz M (1974) Velocity and attenuation of seismic waves in two-phase media. Geophysics 39:587–618
- Mavko G, Mukerji T, Dvorkin J (1998) The rock physics hand book: tools for seismic analysis in a porous media. Cambridge University Press, Cambridge
- Morozov IB (2010) Exact elastic P/SV impedance. Geophysics 75(2):C7–C13
- Ødegaard E, Avseth P (2004) Well log and seismic data analysis using rock physics templates. First Break 23:37–43
- Sayers C (2009) Introduction to this special section-rock physics. Lead Edge 28:15–16
- VerWest B, Masters R, Sena A (2000) Elastic impedance inversion, SEG 2000 Annual Meeting Expanded Abstracts, RC6.8
- Whitcombe DN (2002) Elastic impedance normalisation. Geophysics 67:60–62
- Wijngaarden AV, Jensen SL, Ødegaard E, Avseth P (2004) Seismic reservoir mapping using rock physics templates: example from a North Sea turbidite system. In: EAGE 66th conference and exhibition, Paris

- Xu S, Payne MA (2009) Modelling elastic properties in carbonate rocks. *Lead Edge* 28:66–74
- Xu S, White RE (1995) A new velocity model for clay-sand mixtures. *Geophys Prospect* 43:91–118
- Zhou Z, Hilterman FJ (2010) A comparison between methods that discriminate fluid content in unconsolidated sandstone reservoirs. *Geophysics* 75(1):B47–B58
- Zoeppritz K (1919) Erdbebenwellen VIII B, Ueber Reflexion and Durchgang seismischer Wellen durch Unstetigkeitsflaechen., *Gottinger Nachr.* 1, pp 66–84